ESI Data 1

200/266-nm femtosecond laser ablation system

The LA-ICPMS measurements were performed using a 200/266-nm femtosecond laser ablation (200/266FsLA) system that was developed in-house with OK Laboratory Limited at the Institute for Research on Earth Evolution, Japan Agency for Marine-Earth Science and Technology (IFREE/JAMSTEC), and was manufactured by OK-Fs2000K (OK Laboratory, Tokyo, Japan) (**ESI Data 1 Fig. 1A**). This 200/266FsLA system uses a Solstice one-box Ti: Sapphire femtosecond regenerative amplifier (Spectra-Physics, Santa Clara, CA, USA) with TP-1A THG and TP-1A FHG frequency tripling and quadrupling harmonic generators (Spectra-Physics, Santa Clara, CA, USA). Sets of flip-in mirrors enable co-axial switching between the two different frequency laser beams. Herein, two objective lenses of either excimer laser-grade high-power fused silica (266 nm) or fluorite (200 nm) are used to focus the beams onto the sample surfaces.[1] The two objective lenses are motor driven, and the changeovers are synchronized with the flip-in mirrors. The resulting craters are 30 µm and 90 µm for 200 nm and 266 nm at the maximum sizes, respectively, and can be reduced to 25, 20, 15, 10, and 5 µm for 200 nm and 70, 50, 40, 30, and 15 µm for 266 nm by applying apertures with different diameters. The laser fluences on the sample surface are ~6 J cm^{-2} at 200 nm and ~12 J cm^{-2} at 266 nm **(ESI Data 1 Table 1)**.

Modified sector field mass spectrometer and settings

The 200/266FsLA is coupled to an Element XR sector-field ICPMS (Thermo Fisher Scientific, Bremen, Germany) at the IFREE/JAMSTEC. The Element XR employs both magnetic mass jumps and electrostatic scanning to encompass the mass spectrum range of 6 to 240 amu. Further, the Element XR is equipped with two separate detectors that can be rapidly switched to detect the ion signal from the peak of interest; the detectors include a dual mode secondary electron multiplier (SEM) and a Faraday cup, thereby providing a dynamic range from 0 to 10^{12} cps. The dual mode SEM employs ion counting (0–4 × 10^6 cps) and analogue (10^4–10^9 cps) modes, while the Faraday cup has a range of 10^7–10^{12} cps. Note that daily cross-calibrations of the three detector modes were performed by scanning the ^{38}Ar peak. No mass-dependent fractionation of the detector linearity was observed. However, in this study, the Faraday cup was not used due to the loss of some peak signals in a rapid peak jumping mode.[2] Instead, the detector was forced to use the analogue mode to measure the element peaks with high background and signal intensities (used only for ^{23}Na). This forced analogue mode can provide a dynamic range of 3 × 10^3–4 × 10^9 cps with a reasonably linear response that is well suited to measuring isotopes with a high count rate and background.

In order to obtain an enhanced-sensitivity low oxide molecular SF-ICPMS, we added a high efficiency rotary pump (S60B, Oerlikon Leybold Vacuum, Cologne, Germany) to our Element XR in parallel with the existing expansion rotary pump (UNO35, Pheiffer Vacuum, Asslar, Germany); this led to improvements in the vacuum at the interface—from 2.5 mbar to 1 mbar in solution mode (Ar carrier gas) and to 1.5 mbar in the LA mode (He carrier gas) (**ESI Data 1 Fig. 1B**). We electrically disconnected the guard electrode (GE) shield at the ICP torch and used the normal Ni sampling and Ni skimmer cones (**ESI Data 1 Table 1**). An alternative option is to use cones made from different materials (e.g. Al, Pt),[3] but the conventional normal-Ni cones gave sufficient results, as noted below.

By using the GE, high efficiency X-skimmer, and JET sample cones (Thermo Fischer Scientific, Bremen, Germany)[4] individually, the sensitivity increased by several times; using all of the options together improved the sensitivity by about an order of magnitude in many isotopes.[1, 4, 5] However, the oxide molecular yields, measured as ThO^+/Th^+, was >15% for the solution mode when the normal cyclone nebulizer was used. More than 10% ThO^+/Th^+ was observed even when operating a dry (H_2O solvent free) plasma in the LA mode.[6] Such high oxide molecular yields do not permit the precise determination of elements that have oxide interferences from higher abundance lighter elements (e.g. middle and heavy rare earth elements) in a practical sense.[7] This is particularly true in the case of the LA mode because it is not possible to properly determine the molecular oxide yields unless a set of well-arranged element-doped glass standards are available.[7] Kent and Ungerer (2005) examined the oxide molecular yield in the LA mode by using synthetic glasses and showed that ThO^+/Th^+ < ~2.5% is an acceptable range for the accurate determination of MREEs in most natural sold earth samples.[7] The sizes of molecular oxide interferences were reduced when the ion sampling depth was adjusted by increasing the distance between the ICP torch and sampling cone, and by reducing the sample gas flow.[7-9] However, the signal intensity was also reduced, and the stability of the signal was degraded in our experiments. Even with the 'reduced oxide' setting, it was difficult to achieve ThO^+/Th^+ less than 1% using our SF-ICPMS with the GE-on mode, even when using normal-Ni cones.

In contrast, ThO^+/Th^+ was <0.5% for the solution mode analysis with the normal-Ni cones in the GE-off mode, but instrumental sensitivity was only 0.2 Gcps ppm^{-1} at ^{115}In, which is approximately 10 times less than that at the GE-on mode. After the addition of the high-efficiency rotary pump at the interface (**ESI Data 1 Fig. 1B**), the sensitivity improved to 1.4 Gcps ppm^{-1} in the solution mode when a chilled cyclone splay chamber PC^3 (Elemental Scientific Inc. (ESI), Nebraska, USA) was used; this is comparable to that with the GE-on mode and is realized without causing an increase in the number of oxide molecular ions (ThO^+/Th^+ < 0.5%). When the laser (dry plasma) was used, ThO^+/Th^+ was <0.3%, and signal intensities were 1000–7000 cps ppm^{-1} at 200 nm and 2500–21000 cps ppm^{-1} at 266 nm for the laser crater size of ~30 μm (see details below). We also examined

other interface settings, such as the torch-sample cone distance, sample gas flow, and plasma power. Thus far, for our enhanced sensitivity SF-ICPMS, we have ascertained that our present setting is the most reproducible and stable condition over a period of 18 months (**ESI Data 1 Table 1**).

Sample cell

For LA analysis, the sample was placed in an in-house developed ablation cell with an inner volume of 7 cm^3. Six parallel fine nozzles (diameter 1 mm) generated steady state gas flows inside the cell at >3 cm downstream of the nozzles, and the samples were set within a distance of 3–6 cm downstream. The steady state gas flow was confirmed by (1) a stable ablation, (2) the sensitivity unrelated to the ablation location in the cell, and (3) quick washout of the aerosols, suggesting there were no standing vortexes in the cell. Industrial grade He gas flowed through the cell at a fixed flow rate (1.2 L min^{-1}) to transport the aerosol produced by ablation. We have tested gas blank levels of the isotopes of interest using the industrial grade and the analytical grade gases of both He and Ar; however, no difference was found between the two grades from our supplier. Therefore, we constantly use the industrial grade gases. The He carrier gas with the aerosol flowed into a cylindrical Teflon mixing chamber with an inner volume of 170 cm^3 and mixed with Ar gas (~1 L min^{-1}) just prior to the ICP-torch. The Ar gas flow alone was tuned to achieve a stable optimized signal from the SF-ICPMS.

193ExLA system used for comparison

Along with the 200/266FsLA analyses, a 193-nm excimer (193Ex) LA system (OK-ExLA2000; OK Laboratory, Tokyo, Japan)[5] was also applied. The purpose of this analysis was to provide comparisons between 200/266FsLA and 193ExLA using the same sample cell and SF-ICPMS in order to test the differences of the LA aerosols from the different laser systems. The 193ExLA analyses were performed on SRM612, BHVO-2G, and BCR-2G standard samples and used for determinations of element sensitivity and effect of matrix-induced element fractionation. To achieve this, we used the repetition rate at 10 Hz, laser fluence at the sample surface of ~15 J cm^{-2}, crater diameter at ~30 µm, and analysis using a spot mode. The same rotation raster mode used in the 200/266FsLA (see **ESI Data 2**) is not available with the current 193ExLA system, so we used the spot mode which generated the same crater diameter. Moreover, these analytical conditions of 193ExLA are almost identical to those reported by other researches,[3, 10] so that comparisons to the previous works were also conducted.

Grain size analysis of the laser aerosols

Measurement of the grain size distribution of the laser aerosols from SRM612 and BHVO-2G glasses were made using a Scanning Mobility Particle Sizer SMPS3936L75 (TSI Inc., Minnesota, U.S.A.) at a filtered air flow rate of 0.3 L m^{-1}, and the same laser ablation cell was used with both the 193ExLA and 200/266FsLA systems. The purpose of this was to test the difference in grain size distribution caused by the different laser systems or different matrices, and to examine the effect of grain size distribution on the ionization at the ICP.

References

1. J.-I. Kimura, Q. Chang and K. Tani, *Geochemical Journal*, 2011, **45**, 283-296.
2. M. Humayun, F. A. Davis and M. M. Hirschmann, *Journal of Analytical Atomic Spectrometry*, 2010, **25**, 998-1005.
3. C. Latkoczy and S. Günther, *Journal of Analytical Atomic Spectrometry*, 2002, **17**, 1264-1270.
4. C. Bouman, M. Deerberg, J. B. Schwieters and T. F. Scientific, *Application Note of Thermo Fischer Scientific*, 2008, **30187**, 1-4.
5. J.-I. Kimura, K. Tani and Q. Chang, *Geochemical Journal*, in press.
6. M. Gaboardi and M. Humayun, *Journal of Analytical Atomic Spectrometry*, 2009, **24**, 1188-1197.
7. A. J. R. Kent and C. A. Ungerer, *Journal of Analytical Atomic Spectrometry*, 2005, **20**, 1256-1262.
8. S. Gao, X. Liu, H. Yuan, B. Hattendorf, D. Günther, L. Chen and S. Hu, *Geostandards Newsletter*, 2007, **26**, 181-196.
9. Z. Wang, B. Hattendorf and D. Gunther, *Journal of Analytical Atomic Spectrometry*, 2006, **21**, 1143–1151.
10. Y. Liu, Z. Hu, S. Gao, D. Günther, J. Xu, C. Gao and C. Chen, *Chemical Geology*, 2008, **257**, 34-43.

Table 1. Instrumental setups of 200/266-nm ultraviolet femtosecond laser ablation sector field inductively coupled plasma mass spectrometer (200/266 FsLA-SF-ICPMS)

Laser ablation	
Laser source	800 nm near infrared T-sappire one box regenerative amplifire (Spectra Physics, Solstice)
Wave length	266 nm (frequency tripled by Spectra Physoics, TP-1A THG) 200 nm (frequency quadrupuled by Spectra Physics, TP-1A FHG)
Pulse width	< 300 fs for 200 nm and < 170 fs for 266 nm
Pulse energy	> 300 μJ for 266 nm at laser output > 60 μJ for 200 nm at laser output > 150 μJ for 266 nm at sample surface > 30 μJ for 200 nm at sample surface
Focusing objective lens	THORLABS LMU-UV-193 objective lens for 200 nm Edmund Optics single aspherical objective lens for 266 nm
Beam diameter	5, 10, 15, 20, 25, 30 μm for 200 nm 15, 30, 40, 50, 60, 80 μm for 266 nm
Laser fluence	~6 J cm^{-2} for 200 nm and ~12 J cm^{-2} for 266 nm
Sector field ICP-MS	
SF-ICPMS	Reverse geometry high resolution sector field ICP-MS (Thermo Fisher Scientific, ELEMENT XR)
Plasma power	1.35 kW (27.12 MHz)
Guard electrode	Off (electrically disconnected)
Plasma Ar gas flow rate	13 L min^{-1}
Auxiliary Ar gas flow rate	0.7 L min^{-1}
Sample Ar gas flow rate	1.0 L min^{-1}
Sample He gas flow rate	1.2 L min^{-1}
Sample cone	Normal (Ni)
Skimmer cone	Normal (Ni)
Interface pump	Pfeiffer UNO35 and additional LEYBOLD S60B (total pumping speed 95 m^3 h^{-1})
Interface vacuum	1 - 1.5 mbar with He career gas
Mass resolution	M/ΔM = 400 (low resolution)
Typical sensitivity	1.4 Gcps ppm^{-1} at ^{115}In in solution mode using a Cyclone nebulizer
Oxide molecular	ThO/Th < 0.3 %
Detector mode	Triple or Analog (see text)
Scan speed	~2.6 s per scan

A. 200/266 nm UV femtsecond laser ablation system

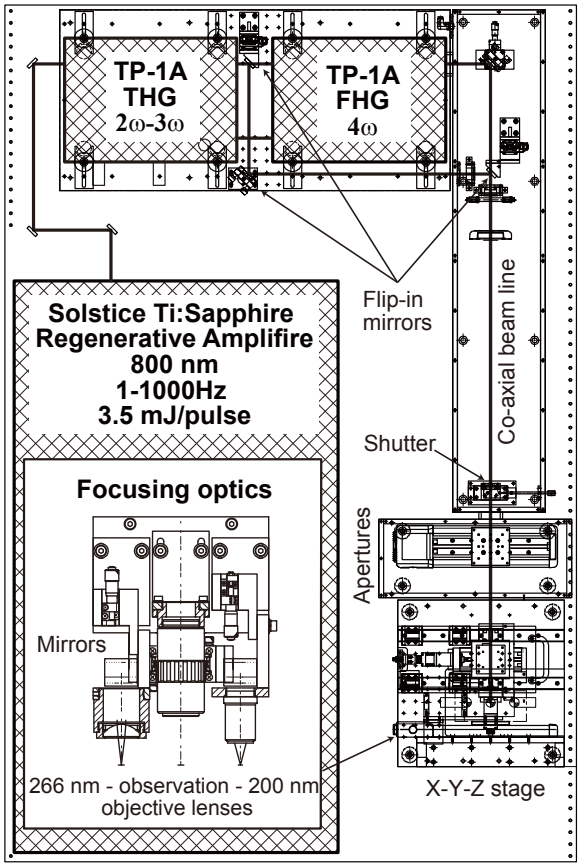

B. Modefied high sensitivity interface of SF-ICPMS

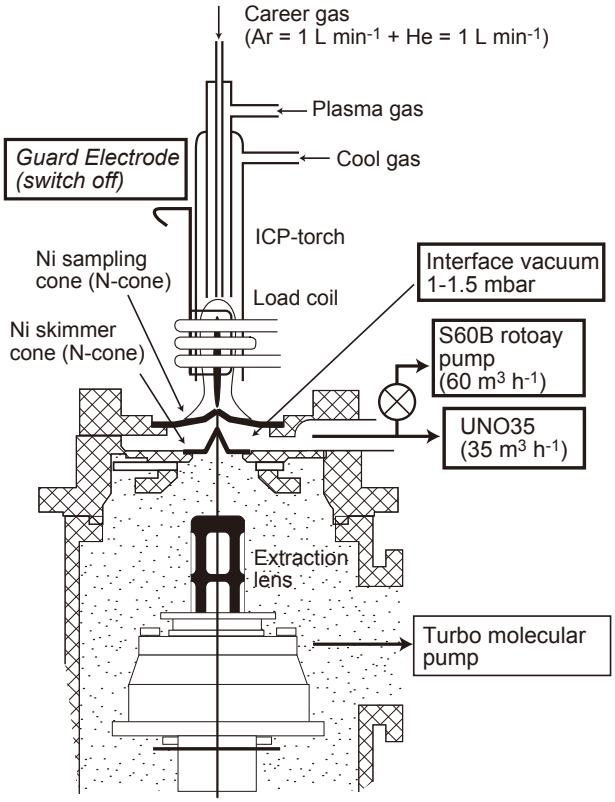

Fig. 1 Schematic pictures of (A) a 200/266-nm femtosecond laser ablation (200/266FsLA) system and (B) a modified interface sector-field inductively coupled plasma mass spectrometer (SF-ICPMS).

ESI Data 2

Rotation raster ablation protocol

Samples were ablated in a rotation raster mode (laser raster along the circumference of a circle with 7 μm radius) with spot sizes of ~15 μm for both 200 nm and 266 nm; the samples were scanned beneath the laser at the rate of 5 μm s^{-1} (**ESI Data 2 Fig. 1A**).[1] The 200FsLA and 266FsLA pulse widths were reportedly <170 fs and <300 fs (Spectra-Physics, personal communication), and all the analyses were performed at a repetition rate of 10 Hz unless otherwise noted. Craters of ~30 μm diameter × ~15 μm depth were created for 200 nm and ~30 μm diameter × ~30 μm depth for 266 nm after 60 s ablation, reflecting the differences in fluence (~6 J cm^{-2} for 200 nm and ~12 J cm^{-2} for 266 nm). The 200-nm mode was principally used, while the 266-nm mode was used for some comparison tests, as indicated in the text.

A circular crater is used for the convenience of creating the greater spatial resolution required in the geological applications. Either line raster or square raster can generate stable signals for accurate analysis; however, adjustment of these crater geometries to the complex texture in the natural geological samples is not always easy. Instead, a circular crater has been useful for most of the high spatial resolution analyses, including small melt inclusions (<30 μm in diameter) in minerals. Therefore, circular spot has been used as the default in many geological LA systems, and we followed this conventional approach. A spot beam analysis, of course, realizes the same spatial resolution. However, the FsLA beam has a Gaussian energy profile, and ablation signals decay quickly[2] due to focused ablation at the crater centre when spot ablation is employed.[3] Homogenization of the FsLA beam is not available because of the ultra-short pulse, which results in optical interferences in the laser beam. The 200/266FsLA signal intensity with 10 Hz repetition rate in spot analyses decrease to about 50% of the initial intensity within 30–60 s.[1, 2] Use of a low repetition rate, such as 1 Hz, can generate prolonged stable signals, but the signal intensity is far below the required level. As a stable ablation signal is the requisite for an accurate determination of element abundances in scanning ICPMS, beam raster is thus essential for FsLA. In order to compromise the crater shape and stable ablation, we have developed the rotation raster protocol. As the result, stable ablation over 60 s is achieved for a crater with ~30 μm diameter (**ESI Data 2 Fig. 1A and B**).[1] Crater shapes were also improved from our previous report[1] by applying a high precision X-Y-Z step motor stage (**ESI Data 2 Fig. 1A and C**) and optimal objective lenses (**ESI Data 2 Fig. 1A** and **ESI Data 1**).

Data acquisition

With SF-ICPMS, all the signals were acquired in the low-resolution mode ($M/\Delta M$ = 400) by peak-jumping between peak-tops with a mass window of 5% and an acquisition time of 50 ms per peak. The mass peaks used for each element are given in **ESI Data 2 Table 1**. The multi-isotope elements were monitored using isotopes that are favourable to ascertain lesser molecular isobaric interference.[4, 5] Isobaric interferences from the sample (^{48}Ca, ^{58}Fe) affect ^{48}Ti and ^{58}Ni, and minor isotopes were used to monitor interferences for these elements. Note that strong doubly charged ion interferences (e.g. $^{47}Ti^{+}$ by $^{94}Zr^{++}$, $^{45}Sc^{+}$ by $^{90}Zr^{++}$) could not be resolved and were substantial for certain minerals (e.g. zircon). These peaks were either not selected ($^{47}Ti^{+}$ by $^{94}Zr^{++}$) or the data were discarded ($^{45}Sc^{+}$ by $^{90}Zr^{++}$). The amount of isobaric interferences from the plasma gas was acquired as a gas blank. All the peaks were acquired by repeatedly sweeping the mass spectrometer in combining six magnet jumps and EScan peak-jumping mode; a single scan from ^{23}Na to ^{238}U took ~2.6 s. Faster scans with shorter settle time and peak acquisition time were available,[6] but those results showed deterioration in the standard deviation of the acquired values. Therefore, the faster scan, which can be used for transient signals such as analysis on fluid inclusions, was not used in this study and is not discussed further.

All the analyses were conducted in the time resolved analysis mode with a time of ~135 s for one spot (**Fig. 1B**). The laser was switched off for the first 20 s after the data acquisition began and was continuously pulsed for the subsequent 60 s. Finally, during the remaining 70 s, the washout sequence of the laser aerosol was measured until the signals returned to the gas blank levels; this normally took 20–30 s after the laser was switched off. Gas blanks were measured before and after the laser signal acquisition during the first and last 20 s, respectively, of the 150 s acquisition. Sample signals were measured in the flat-signal region during 60 s ablation (**ESI Data 2 Fig. 1B**). The background intensities were calculated from the average of the two backgrounds and were subtracted from the peak intensities.

Data processing

The net peak intensities were converted to oxide in wt.% following the method described by Liu *et al.* (2008).[7] As a result, the sum of the concentration of the oxides was 100.00 wt.%, including for cases in which some elements other than normal silicate minerals were the major constituents of the sample (e.g. ZrO_2 and HfO_2 in the case of zircon crystals). This normalization was applicable when the total sum of the 44 analyzed elements were close to 100 wt.%. Involvement of large amounts of halogens (e.g. F and Cl), sulfur (S), and H_2O increased the analytical errors of this method. However, most anhydrous silicate minerals and glasses contain these unanalyzed elements at less than 1 wt.% and thus can be analyzed by this method.[7]

Errors were also propagated from the elements with plural oxidation states (e.g. FeO and

Fe_2O_3); however, resultant errors from the most significant uncertainty in ferric-ferrous iron ratios were less than 10% of the total FeO wt.% (total Fe reported as FeO wt.%), which means that the propagated errors from this uncertainty were less than 1.5% in most cases. The errors are smaller than the typical analytical errors in LA-ICPMS.[7] For convenience, the total sum of the major oxides were presented in this paper as a 100 wt.% basis, with total Fe and Mn reported as FeO and MnO after re-calculations. The total sum of the trace element oxide wt.% were also reported and were always <0.8 wt.% in the silicate glasses and minerals examined in this study. Trace element concentrations were then presented as ppm (see Tables in **ESI Data 4**).

The total sum correction method used was proposed by Guillong *et al.* (2005),[8] and followed by Liu *et al.* (2008).[7] We examined only one single standard,[8] as opposed to using multiple standards with various element concentration levels, as was done by Liu *et al.* (2008) and Gaboardi and Humayun (2009).[4, 7] By using a single standard, the analytical time for the standard and the unknowns was reduced. Even so, in order to minimize the time-dependent drifts,[6, 7] the calibration standard was analyzed between each of five unknown spots. Elemental response factors analyzed by the standards before and after the five unknowns were linearly interpolated to calibrate the concentrations of the unknown samples. All of these designs of the analytical protocol were for the purpose of creating an analysis of a wide range of anhydrous silicate minerals and glasses with a simpler calibration method. With this calibration method, the elemental sensitivities (cps ppm^{-1}) were determined using BHVO-2G as the standard, which was, thus far, found to be ideal (see text).

References

1. J.-I. Kimura, Q. Chang and K. Tani, *Geochemical Journal*, 2011, **45**, 283-296.
2. J. Koch, M. Wälle, J. Pisonero and D. Günther, *Journal of Analytical Atomic Spectrometry*, 2006, **21**, 932-940.
3. R. Freydier, F. Candaudap, F. Poitrasson, A. Arbouet, B. Chatelb and B. Dupré, *Journal of Analytical Atomic Spectrometry*, 2008, **23**, 702-710.
4. M. Gaboardi and M. Humayun, *Journal of Analytical Atomic Spectrometry*, 2009, **24**, 1188-1197.
5. M. Humayun, F. A. Davis and M. M. Hirschmann, *Journal of Analytical Atomic Spectrometry*, 2010, **25**, 998-1005.
6. C. Latkoczy and S. Günther, *Journal of Analytical Atomic Spectrometry*, 2002, **17**, 1264-1270.
7. Y. Liu, Z. Hu, S. Gao, D. Günther, J. Xu, C. Gao and C. Chen, *Chemical Geology*, 2008, **257**, 34-43.
8. M. Guillong, K. Hametner, E. Reusser, S. A. Wilson and D. Günther, *Geostandards and Geoanalytical Research*, 2005, **29**, 315-331.

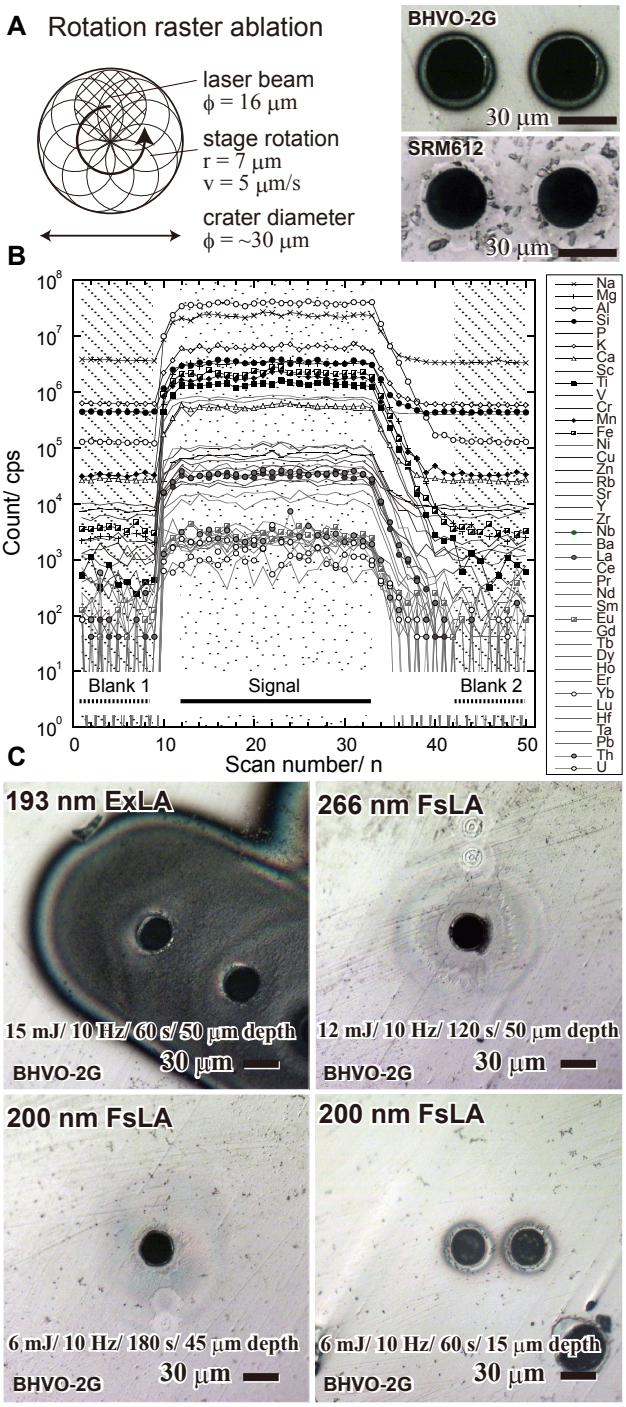

Fig. 1 A laser raster along the circumference of a circle (rotation raster: panel A) generated a crater with steep walls and flatter bottom, resulting in flat and stable signal profiles over 60 s. Typical ablation signal profiles of BHVO-2G glass reference material from USGS are shown in panel B. Gas blanks were measured before and after ablation (blank 1 and blank 2), and signals were acquired as flat regions of the profile (B). Comparison of the deposits around the laser craters generated by 193ExLA, 266FsLA, and 200FsLA at crater size 30 um diameter and about 50 um depth on BHVO-2G are shown in panel C. The 200FsLA craters after 60 s ablation (30 um diameter and 15 um depth) are also shown (panel C). Note that the deposits by 200/266FsLA were far less than those by 193ExLA. Crater photos were taken by a reflected light microscope attached on the OK-FsLA-2000K laser ablation.

Table 1. Elemental responses and lower limits of detection (LLDs) using 200 nm femtosecond laser at 10 Hz rotation raster mode with 30 μm crater

Element	Isotope	Sensitivity (cps ppm^{-1})			LLD (3σ)	unit
		NIST612	NIST610	BHVO-2G		
SiO_2	^{29}Si	786	783	867	0.04	wt.%
TiO_2	^{47}Ti	2780	2250	2950	0.0004	wt.%
Al_2O_3	^{27}Al	1070	1090	1230	0.0002	wt.%
FeO	^{57}Fe	2820	2340	2870	0.001	wt.%
MnO	^{55}Mn	2620	2470	2730	0.00003	wt.%
MgO	^{25}Mg	1520	1560	1710	0.0002	wt.%
CaO	^{42}Ca	2650	2690	2890	0.012	wt.%
Na_2O	^{23}Na	2450	2310	2320	0.04	wt.%
K_2O	^{39}K	3100	4430	3520	0.004	wt.%
P_2O_5	^{31}P	245	339	186	0.001	wt.%
Sc	^{45}Sc	2040	1820	1780	0.20	ppm
V	^{51}V	2980	2730	3250	0.046	ppm
Cr	^{53}Cr	2660	2350	2790	1.16	ppm
Co	^{59}Co	2850	2670	3070	0.094	ppm
Ni	^{60}Ni	2330	2000	2500	9.65	ppm
Cu	^{63}Cu	2320	2250	2360	0.12	ppm
Zn	^{66}Zn	1750	1980	1880	0.15	ppm
Ga	^{71}Ga	4680	4550	4690	0.076	ppm
Rb	^{85}Rb	4310	4220	4470	0.073	ppm
Sr	^{88}Sr	4950	4830	4990	0.034	ppm
Y	^{89}Y	3490	3290	2730	0.022	ppm
Zr	^{90}Zr	3180	3250	2710	0.93	ppm
Nb	^{93}Nb	3770	3340	3510	0.008	ppm
Ba	^{137}Ba	6180	6130	6380	0.094	ppm
La	^{139}La	4710	4860	4760	0.007	ppm
Ce	^{140}Ce	6390	6100	6750	0.006	ppm
Pr	^{141}Pr	6470	6070	6040	0.006	ppm
Nd	^{146}Nd	5670	5650	5470	0.012	ppm
Sm	^{147}Sm	5460	5550	5270	0.017	ppm
Eu	^{153}Eu	6130	6330	6400	0.010	ppm
Gd	^{157}Gd	4910	4700	4190	0.045	ppm
Tb	^{159}Tb	5010	5030	4270	0.003	ppm
Dy	^{163}Dy	4970	4710	4200	0.009	ppm
Ho	^{165}Ho	6150	5750	4850	0.003	ppm
Er	^{166}Er	6180	5800	5250	0.012	ppm
Tm	^{169}Tm	6550	5900	5010	0.006	ppm
Yb	^{172}Yb	6160	5850	5380	0.012	ppm
Lu	^{175}Lu	5780	5220	5100	0.007	ppm
Hf	^{178}Hf	5250	5320	4560	0.007	ppm
Ta	^{181}Ta	5170	4000	4290	0.006	ppm
Pb	^{208}Pb	8490	7720	8540	0.011	ppm
Th	^{232}Th	5350	5110	4840	0.001	ppm
U	^{238}U	7470	7540	8810	0.001	ppm

ESI Data 3

Performance of 200/266FsLA-SF-ICPMS: Sensitivity

We describe herein the basic analytical performance of the 200/266FsLA-SF-ICPMS. First, **ESI Data 3 Fig. 1A** shows the element sensitivity of the system analyzed at 30 μm crater diameters with rotation raster and 10 Hz repetition rate using both 200-nm and 266-nm wavelengths. Resultant crater depths after 60 s ablation were different between the two modes (~15 μm by 200 nm and ~30 μm by 266 nm) because of the difference in the laser fluence (~6 J cm^{-2} and ~12 J cm^{-2}, respectively). Elemental sensitivity therefore differed and was about 2.3 times higher in 266 nm than in 200 nm, reflecting the sampling volume. The apparent elemental sensitivity of 266FsLA was almost identical to that by 193ExLA (**ESI Data 3 Fig. 1A**). However, the depth of the 193FsLA craters after 60 s was ~50 μm; therefore, elemental sensitivity of the 266FsLA is 1.7 to 2.5 times better than in 193ExLA. Due to the lower fluence, the 200FsLA showed about half of the elemental sensitivity (**ESI Data 3 Fig. 1A**). Considering the smaller sampling volume, the elemental sensitivity of the 266FsLA and 200FsLA were almost identical (**ESI Data 3 Fig. 1A**). These levels of sensitivity, however, are still good enough for most of the analyses. The shallower crater penetration (15 μm) into the sample by 200FsLA is preferred for a better spatial resolution.

The enhancement factor by 266FsLA was not as great as in the previous report (8 times), which compared a 266Nd-YAGLA and a 266FsLA, due to the use of a more efficient 193ExLA in this study.[1] The elemental sensitivity was almost comparable to or slightly better than that reported by Latkoczy and Günther (2002) using 193ExLA-SF-ICPMS.[2] Modified SF-ICPMS in this study was almost identical to their facility, apart from the use of normal-Ni sample and skimmer cones, whereas they used Al cones. Latkoczy and Günther (2002) operated a 193ExLA at 10 Hz at 30 μm crater diameter with fluence 15 J cm^{-2}, which is comparable to our 193ExLA. Although it is hard to compare exactly the sampling volume, as the depth of the laser crater was not reported by Latkoczy and Günther (2002), the overall sensitivity of our 193ExLA-SF-ICPMS is identical to their 193ExLA-SF-ICPMS (**ESI Data 3 Fig. 1A**).

Performance of 200/266FsLA-SF-ICPMS: Lower limit of detection

The second basic test was lower limit of detection (LLD). The LLDs were obtained by analyzing standard and gas blank intensities. LLDs were calculated by 3 σ deviations of the elemental concentrations measured from the gas blank intensities (**ESI Data 3 Fig. 1B**). As shown, LLDs by 266FsLA were better than those reported by Latkoczy and Günther (2002). Nearly the same is true even with our 200FsLA, although elemental sensitivity was twice as low as in 266FsLA (**ESI Data 3**

Fig. 1B). This is because of the lower backgrounds obtained by our system, because the elemental sensitivity was almost identical. The only difference which may have affected backgrounds between the two systems was the cone material or impurities in the gases used. It is difficult to do immediate comparisons; however, LLDs of our system are obviously better apart from Na (**ESI Data 3 Fig. 1B**). Comparison is also available to the Liu *et al.* (2008)'s 193ExLA-Q-ICPMS system.[3] The LLDs are almost an order to two orders of magnitude lower, particularly for heavier elements, due to the difference in elemental sensitivities (**ESI Data 3 Fig. 1B**).

Performance of 200/266FsLA-SF-ICPMS: Precision

The third test was the analytical precision represented by the standard deviation of analyzed data. **ESI Data 3 Fig. 2** shows percent standard deviations (% SD) plotted against element concentrations analyzed on the glass reference materials by our 200FsLA-SF-ICPMS, by a 193ExLA-Q-ICPMS by Liu *et al.* (2008),[3] and by a various wavelength (193, 213, and 266 nm) optical parametric oscillator (OPO)-Nd-YAGLA-Q-ICPMS by Guillong *et al.* (2005).[4] The results indicated that analytical precision was almost identical to those reported by Liu *et al.* (2008).[3] In the concentration range between 0.1 ppm to 3000 ppm, the % RDs ranged from <10% to <1%. In the concentration range between 0.008 ppm to 0.1 ppm, the precisions became 10–30% RD. The % RDs by Guillong *et al.* (2005) showed wide variation, mostly <10% RD, irrespective of the concentration levels. Our results were thus almost identical to those reported by Liu *et al.* (2008). Although the sensitivity and LLDs of our system were better than those by Liu *et al.* (2008) (**ESI Data 3 Fig. 1B**), the similar % RDs are from the shorter net acquisition time for an isotope by SF-ICPMS. Notwithstanding improvement of the scan speed in SF-ICPMS,[2] Q-ICPMS provides faster peak jumping with shorter settle time, resulting in longer acquisition time for an isotope during data acquisition. Even so, the performance shown by our 200FsLA-SF-ICPMS is promising, providing the similar counting statistics with those by a high-quality 193ExLA-Q-ICPMS with extended element concentration down to 0.008 ppm.

Overall, our 200/266FsLA-SF-ICPMS showed the best sensitivity by far as compared to that reported by 193ExLA-SF-ICPMS, and the analytical precisions comparable to high-quality 193ExLA-Q-ICPMS data. Moreover, our ion sampling interface gave the lowest LLDs as compared to the previous reports. With these performances of the 200FsLA-SF-ICPMS, we, in this study, investigated the matrix effect induced at the laser ablation site and in the ICP ion source.

Reference

1. J. J. Gonzalez, C. Liu, S.-B. Wen, X. Mao and R. E. Russo, *Talanta*, 2007, **73**, 577-582, doi:510.1016/j.talanta.2007.1004.1028.
2. C. Latkoczy and S. Günther, *Journal of Analytical Atomic Spectrometry*, 2002, **17**,

1264-1270.
3. Y. Liu, Z. Hu, S. Gao, D. Günther, J. Xu, C. Gao and C. Chen, *Chemical Geology*, 2008, **257**, 34-43.
4. M. Guillong, K. Hametner, E. Reusser, S. A. Wilson and D. Günther, *Geostandards and Geoanalytical Research*, 2005, **29**, 315-331.

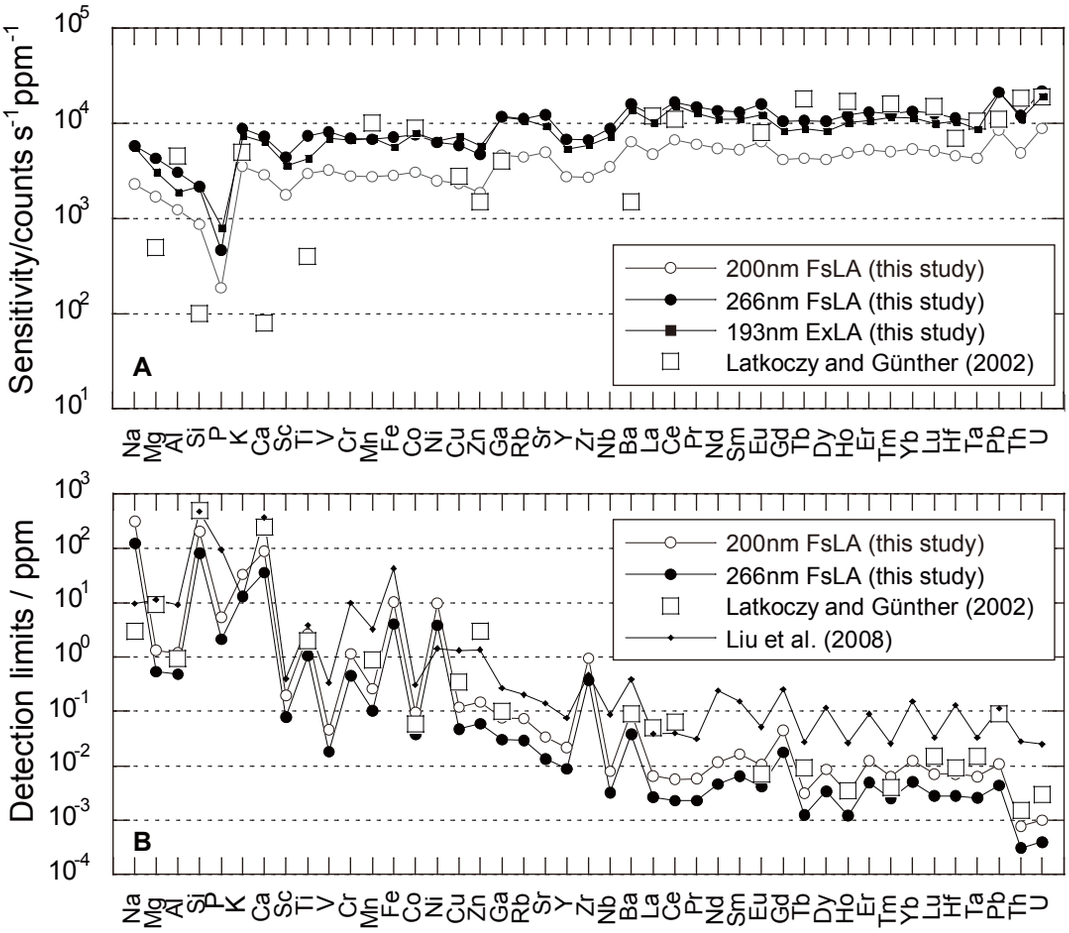

Fig. 1 Elemental responses (panel A) and lower limits of detection (3 σ notation: panel B) of our 200/266Fs-SF-LA-ICPMS and 193Ex-SF-LA-ICPMS in this study, as compared to results from a 193Ex-SF-ICPMS (Latkoczy and Günther, 2002) and a 193ExLA-Q-ICPMS (Liu et al., 2008).

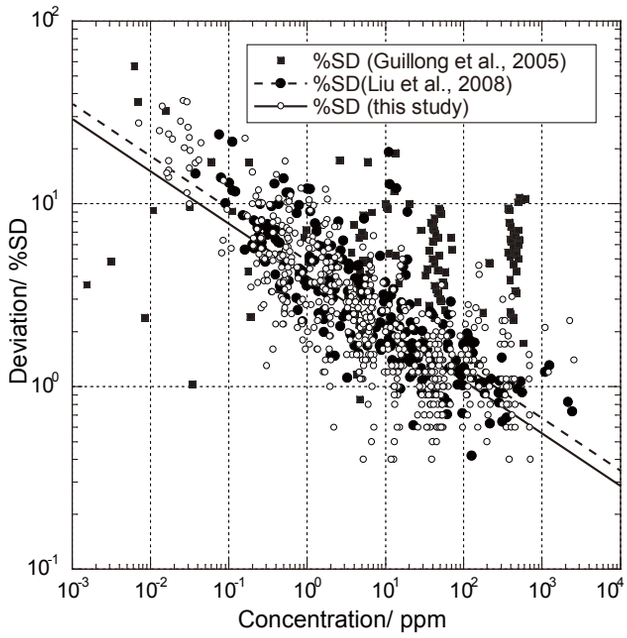

Fig. 2 Deviation of signals measured on USGS and MPI-DING glass reference materials by 200FsLA-SF-ICPMS in comparison to a 193ExLA-Q-ICPMS (Liu et al., 2008) and a various wavelength (193, 213, and 266 nm)

ESI Data 4

Table 1. USGS glass standards analyzed by BHVO-2G and NIST SRM612 as standards under various laser beam conditions

Sample	BCR-2G	BCR-2G			BCR-2G			BCR-2G			BCR-2G			BCR-2G			BCR-2G		
Standard		BHVO-2G			BHVO-2G			BHVO-2G			BHVO-2G			NIST612			NIST612		
FsLA		200 nm			200 nm			266 nm			266 nm			200 nm			266 nm		
Repetition rate		5 Hz			10 Hz			5 Hz			10 Hz			10 Hz			10 Hz		
Crater diameter		30 µm			30 µm			35 µm			35 µm			30 µm			35 µm		
Element	Ref.	AVG	SD%	RD%	AVG	SD%	RD%	AVG	SD%	RD%	AVG	SD%	RD%	AVG	SD%	RD%	AVG	SD%	RD%
SiO_2	55.16	54.10	0.7	-1.9	53.64	0.5	-2.8	55.48	0.7	0.6	54.12	0.6	-1.9	54.43	0.7	-1.3	54.77	0.5	-0.7
TiO_2	2.30	2.36	0.9	2.7	2.40	0.9	4.5	2.30	1.4	0.1	2.36	1.3	2.3	2.54	1.2	10.5	2.61	1.0	13.3
Al_2O_3	13.59	14.61	1.4	7.5	14.33	0.8	5.5	13.86	1.3	2.0	14.20	0.8	4.5	14.36	0.8	5.7	15.07	0.8	10.9
FeO	12.57	12.46	0.9	-0.9	12.78	1.2	1.7	12.15	2.2	-3.4	12.92	1.6	2.7	12.97	1.4	3.1	11.53	1.3	-8.3
MnO	0.19	0.20	1.4	2.2	0.20	1.0	4.0	0.19	2.2	-1.7	0.20	1.2	2.8	0.21	1.5	7.0	0.21	1.3	8.1
MgO	3.61	3.54	1.3	-2.0	3.58	0.4	-0.9	3.39	1.4	-6.2	3.51	1.1	-2.8	3.94	0.6	9.3	4.07	0.5	12.6
CaO	7.16	7.33	0.8	2.4	7.45	0.5	4.1	7.02	0.8	-1.9	7.08	1.3	-1.1	7.24	0.8	1.2	7.42	0.4	3.7
Na_2O	3.28	3.32	0.8	1.5	3.48	0.9	6.2	3.57	2.1	8.9	3.44	1.8	5.1	2.96	1.1	-9.6	3.10	1.8	-5.4
K_2O	1.76	1.70	0.5	-3.4	1.74	0.7	-1.4	1.67	3.2	-5.2	1.78	0.9	1.0	1.12	0.8	-36.7	1.00	1.0	-43.1
P_2O_5	0.38	0.38	1.7	2.2	0.39	0.7	4.3	0.38	1.3	0.6	0.39	1.4	3.7	0.22	0.3	-41.0	0.22	2.4	-40.7
Total	100.00	100.00	0.0		100.00	0.0		100.00	0.0		100.00	0.0		100.00	0.0		100.00	0.0	
ΣTrOx.	0.284	0.282			0.284			0.279			0.280			0.283			0.287		
C.F.		0.87	1.1		0.95	0.8		0.90	1.2		0.94	0.4		0.86	1.1		1.04	0.2	
Sc	33	37.4	0.8	13.4	37.0	0.6	12.1	34.4	1.9	4.4	35.7	1.5	8.2	34.5	0.6	1.4	34.3	0.9	3.8
V	425	402	1.7	-5.4	412	1.1	-3.1	413	3.1	-2.9	405	0.6	-4.7	444	0.6	4.6	445	0.8	4.8
Cr	17.0	15.8	5.7	-6.9	15.5	3.9	-8.7	15.6	4.6	-8.3	15.0	4.0	-11.7	16.3	2.6	-4.0	14.9	5.0	-12.6
Co	38.0	34.7	1.9	-8.6	35.7	0.9	-6.1	35.5	2.5	-6.5	36.0	1.4	-5.2	38.3	1.0	0.8	39.5	1.2	3.9
Ni	13.0	8.91	32.7	-31.5	9.86	28.3	-24.1	10.6	34.7	-18.6	9.10	25.8	-30.0	12.4	15.6	-4.5	14.9	15.3	14.4
Cu	21.0	17.0	1.3	-19.1	17.3	1.6	-17.9	17.1	2.7	-18.4	16.7	1.9	-20.2	15.8	1.7	-24.8	15.3	1.5	-27.0
Zn	125.0	134	1.4	7.0	131	1.2	5.0	142	2.7	13.3	136	2.1	9.1	126	1.1	0.7	115	1.0	-8.2
Ga	23.0	-	-	-	-	-	-	-	-	-	-	-	-	-	-	-	-	-	-
Rb	47.0	46.2	1.4	-1.7	46.6	0.8	-0.9	46.5	2.3	-1.1	48.3	1.3	2.7	45.4	0.7	-3.4	46.0	1.0	-2.2
Sr	342	352	1.0	2.9	351	0.6	2.6	332	2.3	-2.9	339	1.7	-0.7	347	0.9	1.4	362	0.8	5.9
Y	35.0	39.8	0.9	13.6	37.7	0.8	7.7	36.5	1.3	4.4	36.4	0.9	4.0	29.6	1.0	-15.4	32.1	1.2	-8.2
Zr	184	203	0.7	10.3	197	0.5	7.2	189	1.2	2.6	193	1.2	5.0	162	1.0	-11.7	175	0.8	-5.1
Nb	12.5	13.1	1.2	4.8	13.2	0.8	5.4	12.6	3.4	0.4	12.9	1.9	3.5	12.9	0.4	3.5	13.2	0.5	5.6
Ba	683	690	0.7	1.0	701	0.4	2.7	682	1.5	-0.1	691	1.3	1.2	710	1.1	4.0	715	0.6	4.7
La	24.7	26.4	1.2	7.0	26.1	0.6	5.8	24.9	2.3	0.7	25.5	1.5	3.1	24.0	1.3	-2.8	25.7	0.7	4.2
Ce	53.3	53.4	1.0	0.2	54.3	1.4	1.9	51.3	1.9	-3.7	53.2	2.0	-0.2	52.8	0.8	-1.0	54.7	1.0	2.5
Pr	6.7	7.13	1.5	6.4	7.05	0.6	5.3	6.84	2.3	2.1	6.90	1.8	2.9	6.51	2.0	-2.8	6.87	1.0	2.5
Nd	28.9	30.5	1.6	5.7	29.4	2.5	1.5	27.8	1.5	-3.8	29.1	0.8	0.6	27.4	1.0	-5.2	29.3	0.9	1.4
Sm	6.59	6.03	3.4	-8.5	7.32	3.1	11.1	6.43	2.8	-2.4	6.70	2.2	1.6	6.22	2.0	-5.7	6.60	2.4	0.2
Eu	1.97	1.96	4.2	-0.4	1.98	3.1	0.7	2.02	4.5	2.4	2.01	1.4	1.9	1.94	5.7	-1.3	2.11	2.9	7.0
Gd	6.71	6.62	2.4	-1.4	7.15	3.9	6.5	6.64	4.5	-1.0	7.02	1.4	4.6	5.93	3.3	-11.7	6.51	1.5	-3.0
Tb	1.02	1.09	4.4	6.6	1.12	2.8	9.8	1.06	5.7	3.9	1.07	1.7	5.1	0.91	3.0	-11.2	1.00	2.8	-2.4
Dy	6.44	6.88	2.7	6.8	7.00	1.3	8.6	6.26	4.6	-2.7	6.52	3.6	1.3	5.79	2.9	-10.1	6.07	2.1	-5.7
Ho	1.27	1.41	2.4	11.0	1.35	2.3	6.5	1.25	3.7	-1.3	1.34	1.6	5.3	1.14	4.9	-9.9	1.24	2.1	-2.5
Er	3.70	4.22	3.0	14.1	3.93	3.4	6.3	3.54	1.8	-4.4	3.87	3.2	4.6	3.17	2.9	-14.3	3.40	2.4	-7.2
Tm	0.51	0.56	5.8	10.4	0.57	3.5	11.3	0.50	3.8	-1.1	0.60	5.5	16.7	0.44	5.2	-13.5	0.48	5.2	-5.9
Yb	3.39	3.80	3.5	12.0	3.76	1.5	10.8	3.54	3.5	4.4	3.22	3.7	-5.0	3.22	2.7	-4.9	3.35	2.9	-1.1
Lu	0.50	0.60	8.1	19.8	0.51	2.6	1.4	0.52	2.9	3.6	0.51	2.5	1.9	0.44	5.1	-13.3	0.49	2.2	-2.5
Hf	4.84	5.54	3.9	14.4	5.10	5.8	5.3	4.72	2.3	-2.6	4.87	3.3	0.7	4.31	2.9	-11.0	4.85	1.2	0.2
Ta	0.78	0.82	6.1	4.6	0.86	4.2	10.7	0.75	2.1	-3.8	0.81	2.9	4.0	0.72	3.9	-7.3	0.81	2.3	3.4
Pb	11.0	10.6	2.7	-3.5	10.9	1.6	-1.2	10.4	2.6	-5.1	10.8	1.2	-1.7	10.5	1.7	-4.9	9.88	2.0	-10.2
Th	5.90	6.21	3.1	5.3	6.21	1.9	5.2	6.06	2.6	2.7	6.03	0.8	2.1	5.62	1.4	-4.7	6.07	1.7	2.9
U	1.69	1.60	1.2	-5.6	1.66	2.7	-1.5	1.56	3.8	-7.7	1.56	3.4	-7.6	1.69	1.2	0.1	1.73	3.4	2.2

Reference values are from GeoReM; Rep.rate: Repetition rate; Crater dia.: Crater diameter; Ref.: Reference; AVG: Average; SD%: percent one standard deviation; RD%: percent relative deviation; C.F.: Correction factor. Total Fe reported as FeO, ΣTrOx.: total oxide wt.% of trace elements analyzed

Table 1. Continued

Sample	BIR-1G	BIR-1G			BIR-1G			BIR-1G			BIR-1G			BIR-1G			BIR-1G		
Standard		BHVO-2G			BHVO-2G			BHVO-2G			BHVO-2G			NIST612			NIST612		
FsLA		200 nm			200 nm			266 nm			266 nm			200 nm			266 nm		
Repetition rate		5 Hz			10 Hz			5 Hz			10 Hz			10 Hz			10 Hz		
Crater diameter		30 µm			30 µm			35 µm			35 µm			30 µm			35 µm		
Element	Ref.	AVG	SD%	RD%	AVG	SD%	RD%	AVG	SD%	RD%	AVG	SD%	RD%	AVG	SD%	RD%	AVG	SD%	RD%
SiO_2	47.87	46.75	0.8	-2.3	46.76	0.5	-2.3	47.58	1.2	-0.6	46.99	0.6	-1.8	46.91	0.9	-2.0	46.63	0.3	-2.6
TiO_2	1.05	0.96	1.3	-7.9	0.98	1.4	-6.7	0.97	1.4	-7.2	0.94	1.2	-10.0	1.07	1.3	2.5	1.10	1.0	5.1
Al_2O_3	15.62	16.40	1.0	5.0	15.77	0.7	1.0	15.87	1.1	1.6	15.98	0.8	2.3	15.71	1.4	0.6	16.30	0.8	4.3
FeO	10.48	10.47	1.3	-0.1	10.64	0.6	1.6	10.13	1.0	-3.4	10.47	1.3	-0.1	10.13	0.6	-3.3	9.26	0.7	-11.7
MnO	0.19	0.18	2.7	-6.7	0.18	0.9	-7.1	0.18	1.2	-8.5	0.18	0.8	-7.1	0.18	0.7	-7.4	0.18	0.7	-5.9
MgO	9.47	9.53	0.9	0.6	9.69	1.1	2.3	9.68	2.4	2.2	9.71	1.5	2.5	10.68	0.9	12.7	11.05	0.9	16.7
CaO	13.40	13.77	0.9	2.7	14.03	0.3	4.7	13.57	1.6	1.2	13.74	0.5	2.5	13.63	1.0	1.7	13.83	0.8	3.2
Na_2O	1.86	1.89	1.1	1.5	1.90	0.8	1.7	1.98	1.4	6.1	1.93	1.2	3.5	1.67	0.7	-10.6	1.61	0.9	-13.4
K_2O	0.030	0.020	3.0	-35.0	0.020	3.6	-32.6	0.020	1.2	-34.9	0.021	1.3	-31.0	0.012	2.5	-59.3	0.011	1.6	-64.4
P_2O_5	0.027	0.033	3.7	23.0	0.037	3.7	34.6	0.031	3.0	14.3	0.032	1.8	18.0	0.020	3.6	-25.8	0.019	1.3	-29.6
Total	100.00	100.00	0.0		100.00	0.0		100.00	0.0		100.00	0.0		100.00	0.0		100.00	0.0	
ΣTrOx.	0.198	0.187			0.187			0.189			0.187			0.200			0.191		
C.F.		0.99	1.3		1.06	2.9		1.03	1.1		1.02	0.4		0.91	1.5		1.09	0.5	
Sc	43.0	46.5	1.6	8.1	46.5	1.7	8.1	43.7	2.0	1.6	45.5	0.6	5.7	41.9	1.5	-2.4	43.4	0.9	1.0
V	326	310	2.3	-4.8	307	0.8	-5.8	316	3.0	-3.1	305	1.1	-6.5	343	1.1	5.2	325	1.7	-0.2
Cr	392	367	1.9	-6.2	381	1.0	-2.7	382	0.4	-2.7	378	0.8	-3.5	402	1.1	2.5	377	0.7	-3.9
Co	52.0	47.7	1.8	-8.2	49.6	0.6	-4.6	49.1	1.5	-5.6	50.7	0.7	-2.5	54.4	1.2	4.6	53.4	0.8	2.7
Ni	178	157	4.1	-11.9	153	2.3	-14.1	156	4.6	-12.4	162	1.3	-9.0	191	0.9	7.3	182	1.4	2.4
Cu	119	116	1.2	-2.8	116	1.4	-2.5	117	2.5	-2.0	114	1.5	-4.3	115	0.7	-3.5	110	1.4	-7.2
Zn	78.0	71	1.3	-8.5	67.0	1.6	-13.9	72.0	2.5	-7.3	71.0	1.5	-8.5	67.0	2.2	-14.0	60.0	1.9	-23.2
Ga	15.0	-	-	-	-	-	-	-	-	-	-	-	-	14.3	1.8	-	14.2	1.9	-
Rb	0.20	0.16	22.8	-17.7	0.17	8.7	-16.2	0.20	14.9	2.1	0.17	8.6	-12.8	0.22	3.7	13.5	0.19	3.5	-4.0
Sr	109	114	2.8	4.3	111	0.9	1.4	112	1.6	2.7	108	0.9	-0.5	110	0.9	1.3	113	1.2	3.4
Y	14.3	16.4	2.9	14.6	15.7	1.3	10.1	15.5	2.1	8.2	15.3	0.6	6.8	12.2	1.2	-14.4	12.9	1.0	-10.1
Zr	14.00	16	2.4	11.2	14.5	1.2	3.4	14.4	1.0	3.0	14.1	0.6	0.5	12.2	0.4	-13.0	12.5	1.3	-10.5
Nb	0.520	0.545	10.2	4.7	0.538	3.9	3.4	0.549	4.9	5.7	0.552	2.9	6.1	0.527	4.1	1.4	0.548	5.8	5.4
Ba	6.500	7.04	6.7	8.3	6.64	4.3	2.1	6.66	2.7	2.4	6.62	2.3	1.9	6.77	5.2	4.2	7.01	2.9	7.8
La	0.609	0.635	2.5	4.2	0.618	4.6	1.4	0.629	5.1	3.2	0.634	4.8	4.1	0.564	6.5	-7.4	0.597	7.2	-2.0
Ce	1.890	2.00	3.6	5.8	1.95	2.4	3.2	1.96	3.3	3.4	1.95	1.0	3.3	1.91	1.6	1.0	1.95	1.9	3.0
Pr	0.370	0.426	5.0	15.1	0.385	5.3	4.2	0.367	7.9	-0.8	0.395	2.2	6.7	0.354	3.3	-4.2	0.365	3.3	-1.4
Nd	2.370	2.47	7.5	4.4	2.36	3.7	-0.6	2.41	4.5	1.7	2.45	5.2	3.2	2.25	5.1	-5.1	2.40	2.5	1.2
Sm	1.090	1.07	10.1	-1.8	1.21	9.8	11.1	1.05	6.3	-4.2	1.17	6.2	7.6	1.08	10.5	-0.7	1.13	9.2	3.3
Eu	0.517	0.475	7.6	-8.1	0.523	5.6	1.1	0.556	6.7	7.6	0.548	7.4	5.9	0.513	3.7	-0.8	0.535	2.7	3.4
Gd	1.850	1.95	6.8	5.3	1.89	4.3	2.0	1.71	12.0	-7.6	1.69	7.8	-8.6	1.61	4.1	-12.8	1.74	4.4	-6.0
Tb	0.350	0.367	1.6	4.9	0.347	5.1	-0.8	0.363	4.9	3.7	0.366	7.0	4.6	0.312	1.3	-10.9	0.324	3.8	-7.5
Dy	2.550	2.62	5.0	2.6	2.52	4.5	-1.3	2.50	3.6	-2.2	2.44	3.8	-4.2	2.19	3.6	-14.1	2.26	4.0	-11.5
Ho	0.560	0.559	4.9	-0.2	0.580	4.2	3.6	0.584	9.3	4.4	0.585	6.3	4.5	0.468	4.5	-16.5	0.492	2.2	-12.2
Er	1.700	1.83	6.2	7.5	1.75	4.8	3.0	1.60	7.6	-5.7	1.69	2.7	-0.6	1.33	1.6	-21.8	1.49	3.8	-12.4
Tm	0.240	0.262	8.2	9.2	0.262	6.6	9.0	0.238	11.9	-0.7	0.255	6.5	6.3	0.213	11.0	-11.1	0.220	4.7	-8.3
Yb	1.640	1.81	10.6	10.1	1.79	3.0	9.2	1.79	8.2	9.4	1.58	3.5	-3.5	1.45	4.1	-11.4	1.48	5.1	-9.5
Lu	0.248	0.269	5.1	8.4	0.234	8.0	-5.5	0.285	5.0	15.1	0.258	5.7	3.9	0.196	6.5	-21.0	0.222	7.3	-10.7
Hf	0.570	0.588	10.6	3.2	0.587	10.3	3.1	0.613	11.2	7.5	0.565	4.5	-0.9	0.437	10.7	-23.4	0.494	7.0	-13.3
Ta	0.036	0.026	77.0	-28.2	0.026	36.8	-26.8	0.032	19.6	-10.4	0.037	16.7	3.8	0.038	17.4	5.5	0.027	26.2	-24.9
Pb	3.700	3.82	2.8	3.1	3.64	3.3	-1.5	3.52	3.7	-5.0	3.64	3.1	-1.7	3.31	2.0	-10.5	3.10	1.5	-16.2
Th	0.030	0.031	23.1	3.5	0.029	11.5	-2.7	0.031	10.0	4.9	0.031	15.7	4.7	0.030	36.2	-1.1	0.028	20.2	-8.3
U	0.023	0.014	34.1	-39.6	0.017	15.3	-26.8	0.017	24.1	-25.6	0.017	14.0	-24.0	0.015	14.8	-35.5	0.015	17.2	-32.9

Reference values are from GeoReM; Rep.rate: Repetition rate; Crater dia.: Crater diameter; Ref.: Reference; AVG: Average; SD%: percent one standard deviation; RD%: percent relative deviation; C.F.: Correction factor. Total Fe reported as FeO, ΣTrOx.: total oxide wt.% of trace elements analyzed

Table 2. MPI-DING synthetic glass standards analyzed by BHVO-2G as the standard under recommended laser beam conditions

Sample	GOR128G	GOR128G			GOR132G	GOR132G			GSC-1G	GSC-1G			GSD-1G	GSD-1G			KL2-G	KL2-G		
Standard		BHVO-2G				BHVO-2G				BHVO-2G				BHVO-2G				BHVO-2G		
FsLA		200 nm				200 nm				200 nm				200 nm				200 nm		
Repetition rate		10 Hz				10 Hz				10 Hz				10 Hz				10 Hz		
Crater diameter		30 μm				30 μm				30 μm				30 μm				30 μm		
Element	Ref.	AVG	SD%	RD%	Ref.	AVG	SD%	RD%	Ref.	AVG	SD%	RD%	Ref.	AVG	SD%	RD%	Ref.	AVG	SD%	RD%
SiO_2	46.49	46.94	1.2	1.0	46.05	46.18	0.3	0.3	53.23	52.51	0.2	-1.3	53.86	52.97	0.3	-1.7	51.16	51.29	0.4	0.3
TiO_2	0.29	0.25	0.3	-12.6	0.31	0.28	1.4	-11.1	1.39	1.40	0.6	0.9	1.26	1.26	0.5	0.6	2.60	2.55	0.6	-2.2
Al_2O_3	9.99	9.38	0.9	-6.1	11.13	10.68	1.6	-4.1	13.66	14.48	0.4	6.0	13.57	14.42	0.6	6.3	13.53	13.06	1.0	-3.4
FeO	9.89	10.90	2.3	10.2	10.22	11.06	1.1	8.2	13.86	13.59	0.7	-2.0	13.47	13.17	0.7	-2.2	10.88	11.36	1.1	4.4
MnO	0.18	0.19	2.6	5.8	0.16	0.16	0.4	4.7	0.02	0.02	0.7	0.4	0.03	0.03	0.7	-5.1	0.17	0.17	0.8	1.4
MgO	26.22	25.71	1.0	-1.9	22.67	22.41	0.4	-1.1	3.64	3.58	0.7	-1.7	3.64	3.59	0.6	-1.4	7.46	7.27	1.2	-2.6
CaO	6.29	5.88	1.1	-6.6	8.55	8.22	0.7	-3.8	7.18	7.24	0.3	0.8	7.29	7.20	0.9	-1.2	11.09	10.94	1.0	-1.3
Na_2O	0.58	0.67	1.4	16.1	0.84	0.93	1.3	10.4	3.64	3.84	1.1	5.3	3.64	3.99	0.6	9.5	2.39	2.56	0.7	7.1
K_2O	0.04	0.04	2.3	3.3	0.03	0.03	2.8	5.5	3.13	3.04	0.8	-2.9	3.04	3.11	0.7	2.3	0.49	0.51	0.8	5.1
P_2O_5	0.03	0.03	3.6	33.5	0.04	0.04	1.3	13.7	0.23	0.29	0.5	27.2	0.20	0.24	1.0	22.7	0.24	0.29	1.4	22.1
Total	100.00	100.00	0.0		100.00	100.00	0.0		100.00	100.00	0.0		100.00	100.00	0.0		100.00	100.00	0.0	
ΣTrOx.	0.545	0.544			0.621	0.630			0.034	0.033			0.189	0.193			0.245	0.244		
C.F.		1.22	2.7			1.16	3.5			0.98	1.1			1.00	1.3			1.06	1.1	
Sc	32.1	32.6	0.9	1.6	36.5	37.4	1.7	2.5	5.40	6.09	1.5	12.7	52.0	54.4	0.6	4.6	31.8	32.1	1.2	0.8
V	189	185	2.1	-1.9	214	219	0.8	2.1	5.40	4.76	2.1	-11.9	44.0	38.8	0.4	-11.8	309	317	2.0	2.4
Cr	2272	2253	2.3	-0.8	2528	2556	1.4	1.1	10.3	9.29	3.7	-9.8	42.0	40.6	1.9	-3.3	294	290	1.7	-1.3
Co	92.4	92.8	1.5	0.4	92.7	96.9	0.6	4.5	5.90	5.57	1.9	-5.5	40.0	36.8	0.7	-8.0	41.2	43.0	1.7	4.4
Ni	1074	1094	2.1	1.9	1187	1214	1.2	2.3	21.0	18.5	8.6	-12.2	58.0	52.0	3.6	-10.3	112	105	2.2	-6.2
Cu	63.8	66.8	1.3	4.7	205	213	1.0	4.1	16.0	13.6	1.3	-14.9	42.0	39.8	0.5	-5.2	87.9	89.9	1.9	2.3
Zn	74.7	69.5	1.3	-7.0	76.8	63.0	1.0	-18.0	12.7	11.6	2.1	-9.0	54.0	47.9	1.7	-11.3	110	105	1.6	-4.5
Ga	8.67	9.31	1.6	7.4	10.4	11.2	2.8	7.9	10.0	9.72	1.2	-2.8	54.0	53.8	0.6	-0.5	20.0	22.0	1.2	9.9
Rb	0.41	0.41	8.1	2.1	2.10	2.18	0.6	3.6	4.92	4.90	1.1	-0.4	37.3	38.0	1.3	2.0	8.7	9.06	2.6	4.2
Sr	30.0	28.1	1.0	-6.3	15.3	14.3	0.9	-6.4	32.3	31.4	0.7	-2.9	69.4	67.5	0.8	-2.8	356	352	1.0	-1.3
Y	11.8	12.8	1.0	8.7	12.9	14.1	1.1	9.5	4.80	5.13	1.1	6.9	42.0	46.4	1.1	10.5	25.4	26.0	1.7	2.2
Zr	10.0	10.5	2.1	4.5	9.90	10.4	2.1	4.9	6.80	6.64	0.5	-2.3	42.0	44.8	1.0	6.6	152	151	0.6	-0.5
Nb	0.10	0.09	13.4	-13.9	0.073	0.059	48.1	-19.7	4.50	4.88	1.1	8.4	42.0	45.7	0.9	8.7	15.0	14.8	1.6	-1.1
Ba	1.06	1.11	3.7	4.9	0.815	0.834	12.2	2.3	34.8	34.8	1.2	0.0	67.0	69.0	1.2	2.9	123	120	0.8	-1.8
La	0.121	0.107	5.7	-11.4	0.084	0.081	5.4	-3.6	4.36	4.52	1.5	3.7	39.1	40.3	1.1	3.2	13.1	13.0	0.9	-1.1
Ce	0.450	0.448	3.7	-0.5	0.393	0.403	14.5	2.5	4.62	4.62	1.7	-0.1	41.4	41.2	0.8	-0.4	32.4	33. 5	0.6	3.2
Pr	0.100	0.094	9.3	-5.6	0.089	0.084	6.3	-5.6	4.80	4.93	1.1	2.8	45.0	48.1	1.1	6.9	4.60	4.67	1.2	1.4
Nd	0.784	0.739	4.5	-5.8	0.689	0.702	6.9	1.9	4.72	4.75	1.5	0.6	44.7	45.6	0.6	2.0	21.6	21.8	2.1	1.0
Sm	0.525	0.520	17.1	-0.9	0.508	0.494	3.8	-2.7	5.00	5.06	1.4	1.2	47.8	48.8	0.6	2.2	5.54	5.45	2.5	-1.5
Eu	0.264	0.266	10.1	0.8	0.255	0.261	8.1	2.4	4.40	4.51	1.9	2.4	41.0	43.0	0.9	4.8	1.92	1.98	1.9	3.3
Gd	1.17	1.19	5.7	1.3	1.19	1.17	6.6	-1.7	5.29	5.34	2.9	1.0	50.7	52.1	1.4	2.8	5.92	5.70	2.4	-3.7
Tb	0.248	0.257	2.7	3.5	0.269	0.283	3.8	5.4	5.10	5.20	0.4	1.9	47.0	51.6	0.6	9.8	0.89	0.87	2.2	-2.8
Dy	1.98	1.98	4.8	0.2	2.15	2.24	7.5	4.0	5.41	5.90	2.3	9.1	51.2	56.2	1.0	9.8	5.22	5.22	2.2	-0.1
Ho	0.443	0.470	3.1	6.2	0.507	0.518	3.4	2.2	5.10	5.24	1.3	2.7	49.0	52.9	0.7	8.0	0.96	0.94	1.6	-2.1
Er	1.40	1.41	2.9	0.9	1.56	1.73	1.4	10.4	3.72	3.98	3.1	7.1	40.1	42.6	1.2	6.2	2.54	2.58	3.7	1.4
Tm	0.204	0.199	10.0	-2.6	0.234	0.242	5.3	3.6	5.20	5.78	1.4	11.2	49.0	56.6	1.1	15.6	0.33	0.33	5.3	-1.1
Yb	1.41	1.34	5.9	-5.1	1.61	1.61	5.5	0.3	5.29	5.51	3.6	4.1	50.9	51.0	0.9	0.2	2.10	2.06	2.6	-1.9
Lu	0.206	0.205	5.9	-0.7	0.237	0.240	10.1	1.3	5.33	5.51	1.8	3.4	51.5	53.4	0.7	3.7	0.29	0.28	2.8	-2.5
Hf	0.349	0.331	9.9	-5.1	0.357	0.368	8.6	2.9	4.30	4.49	2.7	4.5	39.0	41.8	1.0	7.1	3.93	3.92	2.5	-0.4
Ta	0.019	0.019	22.6	-1.5	0.031	0.024	28.3	-24.1	4.40	4.77	1.1	8.4	40.0	45.2	0.5	12.9	0.96	0.87	1.8	-9.0
Pb	0.345	0.305	4.1	-11.5	19.5	19.2	2.7	-1.4	14.0	13.5	2.2	-3.3	50.0	49.2	1.4	-1.7	2.07	2.01	2.2	-3.0
Th	0.008	0.007	27.7	-13.0	0.009	0.009	98.5	3.7	4.20	3.93	2.3	-6.4	41.0	43.3	1.1	5.5	1.02	1.01	2.0	-1.1
U	0.012	0.013	25.2	4.0	0.048	0.044	21.6	-7.4	4.70	4.30	1.5	-8.5	41.0	39.3	1.3	-4.1	0.55	0.49	3.0	-10.5

Reference values are from GeoReM; Rep.rate: Repetition rate; Crater dia.: Crater diameter; Ref.: Reference; AVG: Average; SD%: percent one standard deviation; RD%: percent relative deviation; C.F.: Correction factor. Total Fe reported as FeO, ΣTrOx.: total oxide wt.% of trace elements analyzed

Table 2. Continued

Sample	ML3B-G	ML3B-G			TB-1G	TB-1G			StHs680-G	StHs680-G			ATHO-G	ATHO-G		
Standard		BHVO-2G				BHVO-2G				BHVO-2G				BHVO-2G		
FsLA		200 nm				200 nm				200 nm				200 nm		
Repetition rate		10 Hz				10 Hz				10 Hz				10 Hz		
Crater diameter		30 µm				30 µm				30 µm				30 µm		
Elem.	Ref.	AVG	SD%	RD%	Ref.	AVG	SD%	RD%	Ref.	AVG	SD%	RD%	Ref.	AVG	SD%	RD%
SiO_2	52.29	52.38	0.7	0.2	54.91	54.29	0.5	-1.1	63.83	63.34	0.3	-0.8	75.87	74.23	0.3	-2.2
TiO_2	2.17	2.07	1.1	-4.5	0.86	0.84	0.9	-2.4	0.70	0.67	0.6	-5.2	0.26	0.24	0.7	-4.7
Al_2O_3	13.83	13.57	0.7	-1.9	16.89	17.12	0.7	1.4	17.84	17.84	0.8	0.0	12.24	12.53	0.6	2.4
FeO	11.09	11.62	2.3	4.8	8.25	8.67	1.4	5.1	4.38	4.56	0.7	4.1	3.28	3.51	1.4	7.1
MnO	0.17	0.18	2.0	1.4	0.19	0.18	1.0	-1.0	0.08	0.07	1.2	-2.6	0.11	0.11	0.9	0.8
MgO	6.70	6.49	0.9	-3.2	3.69	3.51	1.0	-4.8	1.97	1.82	0.8	-7.8	0.10	0.09	0.8	-16.1
CaO	10.68	10.36	1.1	-3.0	6.96	6.70	0.5	-3.7	5.29	4.97	1.4	-6.0	1.71	1.59	1.5	-6.7
Na_2O	2.44	2.69	1.7	10.0	3.24	3.56	2.4	9.7	4.45	5.21	1.0	17.2	3.76	4.86	1.3	29.1
K_2O	0.39	0.40	2.0	1.7	4.43	4.52	1.1	2.2	1.29	1.33	0.9	3.3	2.65	2.80	1.0	5.6
P_2O_5	0.23	0.25	2.0	7.7	0.60	0.61	1.1	1.9	0.16	0.17	1.3	4.7	0.03	0.03	3.5	38.0
Total	100.00	100.00	0.0		100.00	100.00	0.0		100.00	100.00	0.0		100.00	100.00	0.0	
ΣTrOx.	0.204	0.207			0.427	0.426			0.163	0.156			0.240	0.244		
C.F.		1.10	0.6			1.03	1.5			1.22	1.4			1.10	2.7	
Sc	31.6	30.7	1.5	-2.9	22.8	23.0	0.6	0.8	11.5	10.8	3.1	-6.2	7.00	7.67	1.3	9.5
V	268	287	1.9	7.2	189.2	179	1.3	-5.5	90.3	82.4	1.5	-8.8	3.91	3.24	2.8	-17.2
Cr	177	164	2.7	-7.4	60.0	55.8	3.0	-7.1	16.9	12.5	9.6	-26.3	6.10	4.15	18.3	-32.0
Co	41.2	43.1	0.8	4.6	23.5	22.8	0.2	-3.2	13.2	12.5	1.7	-5.6	2.13	1.27	2.5	-40.3
Ni	107	104	2.6	-3.0	19.4	14.5	6.5	-25.5	23.7	19.8	5.7	-16.7	13.0	5.97	34.0	-54.1
Cu	112	115	1.7	3.0	73.1	76.1	1.0	4.1	41.5	37.4	2.7	-9.9	18.6	18.7	1.4	0.3
Zn	108	108	1.8	-0.1	102.3	106	2.0	4.0	67.0	56.7	1.6	-15.4	141	137	1.5	-3.1
Ga	19.6	21.0	1.4	7.3	19.8	23.6	1.4	19.1	20.9	21.1	1.7	1.0	25.3	27.2	1.3	7.6
Rb	5.80	6.12	3.0	5.5	144.7	150	1.2	4.2	30.7	30.1	1.1	-2.0	65.3	66.4	1.2	1.7
Sr	312	311	1.7	-0.4	1363	1315	1.4	-3.5	482	466	1.0	-3.4	94.1	86.3	1.3	-8.3
Y	23.9	24.7	1.5	3.2	26.9	26.4	1.6	-1.9	11.4	11.9	1.7	4.0	94.5	106	1.5	12.1
Zr	122	125	1.0	2.8	250	245	2.2	-2.0	118	122	1.7	3.1	512	565	1.5	10.3
Nb	8.61	8.54	3.2	-0.8	28.2	29.8	1.2	5.5	6.94	6.81	2.1	-1.8	62.4	64.1	1.8	2.7
Ba	80.1	80.2	1.0	0.1	924.9	976	1.5	5.6	298	293	1.6	-1.7	547	526	1.6	-3.8
La	8.99	9.08	0.8	1.0	45.3	44.1	1.1	-2.7	12.0	11.5	2.2	-4.1	55.6	54.7	1.5	-1.7
Ce	23.1	23.3	0.9	2.1	89.7	92.0	1.7	2.1	26.1	25.4	1.2	-2.6	121	121	2.1	-0.2
Pr	3.43	3.45	1.0	0.7	10.6	10.7	1.8	1.4	3.20	3.09	1.1	-3.5	14.6	14.7	1.7	0.7
Nd	16.7	16.6	1.4	-0.6	40.0	40.1	2.9	1.4	13.0	12.7	2.5	-2.1	60.9	61.3	1.0	0.7
Sm	4.75	4.90	4.8	3.2	7.63	7.23	2.6	-5.2	2.78	2.68	4.7	-3.6	14.2	14.2	2.2	-0.3
Eu	1.67	1.72	2.9	2.9	1.91	1.81	3.7	-5.4	0.95	0.89	1.3	-6.1	2.76	2.73	1.1	-1.0
Gd	5.26	5.25	3.7	-0.3	6.20	5.79	3.8	-6.7	2.59	2.48	5.1	-4.3	15.3	15.3	2.5	0.2
Tb	0.80	0.81	3.6	1.7	0.84	0.78	3.3	-6.8	0.37	0.35	2.3	-5.2	2.51	2.70	2.1	7.4
Dy	4.84	4.94	2.3	2.1	4.95	4.79	1.8	-3.2	2.22	2.09	6.2	-5.9	16.2	17.4	1.3	7.5
Ho	0.91	0.92	3.1	1.7	0.98	0.90	3.7	-7.9	0.42	0.43	3.2	1.5	3.43	3.80	1.5	10.7
Er	2.44	2.42	4.0	-0.7	2.76	2.67	5.0	-3.2	1.18	1.19	6.0	1.1	10.3	11.7	2.4	13.5
Tm	0.32	0.32	2.3	0.3	0.39	0.41	3.8	4.4	0.17	0.18	7.0	1.8	1.52	1.63	1.9	7.4
Yb	2.06	1.95	3.6	-5.5	2.58	2.64	4.7	2.4	1.13	1.10	7.5	-3.1	10.5	10.8	2.9	2.8
Lu	0.29	0.29	4.6	-0.2	0.40	0.39	6.4	-3.4	0.17	0.17	6.5	0.5	1.54	1.71	2.8	10.9
Hf	3.22	3.23	3.6	0.4	5.87	5.93	2.4	1.0	3.07	3.06	2.7	-0.3	13.7	14.9	1.5	8.8
Ta	0.56	0.54	3.3	-1.9	1.51	1.60	4.3	6.1	0.42	0.40	2.2	-4.2	3.90	4.10	1.1	5.1
Pb	1.38	1.34	6.4	-2.8	16.0	16.8	1.2	5.0	10.3	10.0	1.7	-2.9	5.67	5.69	2.2	0.3
Th	0.55	0.54	2.5	-2.3	15.0	15.1	2.2	0.5	2.28	2.24	2.3	-1.8	7.40	7.68	1.8	3.8
U	0.44	0.46	3.8	4.0	4.20	4.11	2.5	-2.0	1.01	0.91	2.8	-10.0	2.37	2.16	3.3	-8.9

Reference values are from GeoReM; Rep.rate: Repetition rate; Crater dia.: Crater diameter; Ref.: Reference; AVG: Average; SD%: percent one standard deviation; RD%: percent relative deviation; C.F.: Correction factor. Total Fe reported as FeO, ΣTrOx.: total oxide wt.% of trace elements analyzed

Table 3. Analytical results for plagioclase, clinopyroxene, garnet, and zircon crystals

Sample	MK-1	MK-1			SAE113	SAE113			SAE113	SAE113			Sample	91500	91500			91500		
	Plagioclase				Clinopyroxene				Garnet					Zircon						
Standard		BHVO-2G				BHVO-2G				BHVO-2G			Standard		SRM610			BHVO-2G		
FsLA		200 nm				200 nm				200 nm			FsLA		200 nm			200 nm		
Repetition rate		10 Hz				10 Hz				10 Hz			Repetition rate		10 Hz			10 Hz		
Crater diameter		30 µm				30 µm				30 µm			Crater diameter		30 µm			30µm		
Element	Ref.	AVG	SD%	RD%	Ref.	AVG	SD%	RD%	Ref.	AVG	SD%	RD%	Element	Ref.	AVG	SD%	RD%	AVG	SD%	RD%
SiO_2	44.50	42.34	0.8	-4.8	54.08	52.62	0.7	-2.7	41.48	41.59	0.7	0.3	SiO2	34.15	32.55	0.6	-4.7	26.89	1.3	-21.3
TiO_2	0.011	0.007	5.9	-29.8	0.46	0.42	1.1	-9.3	0.39	0.40	0.8	2.1	ZrO2	65.16	66.71	0.4	2.4	72.42	0.5	11.2
Al_2O_3	34.91	36.57	1.4	4.7	6.05	5.80	1.8	-4.1	23.40	23.20	0.7	-0.9	HfO2	0.685	0.643	9.5	-6.1	0.62	1.6	-8.9
FeO	0.46	0.48	2.0	3.9	5.91	6.20	2.3	4.8	9.96	10.18	0.9	2.3	TiO2	0.0010	0.0008	64.2	-20.8	0.0005	12.4	-46.0
MnO	0.007	0.00	11.5	-44.0	0.14	0.14	1.2	-5.4	0.28	0.28	2.3	1.4	MnO	-	0.0001	85.7	-	-	-	-
MgO	0.10	0.11	5.4	8.1	17.93	17.66	0.8	-1.5	20.10	19.66	0.8	-2.2	MgO	-	0.0012	86.6	-	-	-	-
CaO	19.52	19.84	1.5	1.7	13.58	15.06	0.5	10.9	4.36	4.56	2.2	4.6	CaO	-	0.0308	80.9	-	0.0267	78.0	-
Na_2O	0.49	0.59	6.1	18.7	1.83	2.06	1.6	12.4	0.04	0.06	7.6	38.0	Na2O	-	0.0208	30.2	-	0.0259	78.0	-
K_2O	0.006	0.007	56.8	17.1	0.013	0.015	4.2	19.7	-	0.001			K2O	-	0.0042	76.9	-	0.0002	217	-
P_2O_5	-	0.06	-	-	-	0.02	7.3		-	0.07	18.1		P2O5	0.0055	0.0419	20.1	661	0.0118	3.6	115
Total	100.00	100.00			100.00	100.00			100.00	100.00			Total	100.00	100.00			100.00		
ΣTrOx.	0.038	0.039			0.289	0.429			0.472	0.594				0.793	0.694			0.71	0.659	
C.F.		1.48				0.97				1.08					0.70					
Sc	0.11	-	-	-	-	21.94	1.2	-	-	94.5	7.2	-	Sc	-	-	-	-	-	-	-
V	-	-	-	-	-	255	1.9	-	-	164	4.6	-	V	-	-	-	-	-	-	-
Cr	-	-	-	-	1886	2074	2.5	10.0	3141	3521	6.9	12.1	Cr	1.50	-	-	-	0.45	106	-69.9
Co	2.50	-	-	-	-	41.05	2.2	-	-	53.4	1.4	-	Co	-	-	-	-	-	-	-
Ni	8.37	-	-	-	-	398.09	2.8	-	-	81.5	1.7	-	Ni	0.070	-	-	-	-	-	-
Cu	1.80	-	-	-	-	3.39	20.7	-	-	0.340	30.4	-	Cu	-	-	-	-	-	-	-
Zn	-	-	-	-	-	42.6	4.0	-	-	33.9	3.6	-	Zn	-	-	-	-	-	-	-
Ga	-	-	-	-	-	9.51	3.4	-	-	8.00	1.4	-	Ga	-	-	-	-	-	-	-
Rb	0.07	-	-	-	0.005	0.014	69.6	184.2	0.0004	0.0290	51.6	7150	Rb	-	0.28	105	-	0.06	16.2	-
Sr	305	321	3.2	5.3	76.9	76.7	1.5	-0.2	0.435	0.569	61.1	30.8	Sr	0.05	0.20	68.7	294	0.14	11.9	186
Y	-	-	-	-	6.04	6.06	2.1	0.4	41.2	38.5	2.0	-6.6	Y	140	139	4.0	-1.0	136	2.9	-3.2
Zr	-	-	-	-	16.00	16.5	2.8	3.4	37.1	34.6	1.0	-6.6	Zr	-	-	-	-	-	-	-
Nb	-	-	-	-	0.252	0.104	3.0	-58.9	0.048	0.051	13.8	6.3	Nb	0.790	1.026	6.4	29.9	0.925	2.0	17.1
Ba	6.28	6.80	3.4	8.3	0.396	0.149	58.4	-62.3	0.115	0.000	8773	-99.6	Ba	0.060	-	-	-	-	-	-
La	0.034	0.041	8.3	21.8	0.844	0.976	1.7	15.7	0.014	0.015	41.7	9.9	La	0.0060	0.0065	79.1	7.8	0.0035	66.0	-41.1
Ce	0.074	0.086	1.3	15.6	3.310	3.751	1.5	13.3	0.180	0.196	0.4	8.9	Ce	2.60	2.68	7.7	3.2	2.01	3.0	-22.8
Pr	0.009	0.016	16.7	81.2	0.702	0.749	2.6	6.7	0.083	0.078	3.3	-6.4	Pr	0.024	0.008	222	-68.0	0.010	40.6	-58.7
Nd	0.066	0.065	10.4	-1.8	4.290	4.274	0.8	-0.4	0.905	0.859	0.8	-5.1	Nd	0.240	0.18	74.0	-24.3	0.16	19.3	-38.0
Sm	0.011	0.020	197	79.5	1.380	1.395	4.4	1.1	0.940	0.899	10.0	-4.4	Sm	0.50	0.45	20.8	-10.5	0.37	12.6	-26.8
Eu	0.063	0.070	18.9	11.6	0.428	0.501	4.6	17.0	0.511	0.502	2.5	-1.8	Eu	0.24	0.23	33.3	-3.4	0.19	6.1	-19.9
Gd	-	-	-	-	1.340	1.567	7.7	16.9	2.340	2.46	4.8	5.3	Gd	2.20	1.77	7.4	-19.4	1.95	8.7	-11.5
Tb	-	-	-	-	0.213	0.232	1.4	9.1	0.623	0.598	2.4	-4.0	Tb	0.86	0.87	11.1	1.0	0.76	4.8	-11.4
Dy	-	-	-	-	1.220	1.289	2.5	5.7	5.560	5.22	2.7	-6.0	Dy	12.0	11.7	3.9	-2.3	10.9	3.6	-9.0
Ho	-	-	-	-	0.216	0.227	2.0	5.2	1.440	1.369	1.6	-4.9	Ho	4.80	4.81	3.2	0.3	4.58	4.3	-5.1
Er	-	-	-	-	0.523	0.572	3.1	9.4	4.790	4.89	3.5	2.2	Er	25.0	24.5	5.4	-2.0	25.1	3.2	0.4
Tm	-	-	-	-	0.073	0.078	7.3	6.3	0.880	0.856	6.5	-2.7	Tm	6.90	6.64	4.2	-3.7	6.93	2.4	0.5
Yb	-	-	-	-	0.390	0.424	4.0	8.6	6.450	6.47	3.7	0.3	Yb	74.0	79.0	3.0	6.7	73.8	2.1	-0.2
Lu	-	-	-	-	0.058	0.054	8.1	-7.4	1.070	1.07	6.8	-0.5	Lu	13.0	12.1	3.4	-7.0	10.8	2.0	-16.9
Hf	-	-	-	-	0.706	0.731	4.1	3.6	0.757	0.705	3.1	-6.9	Hf	5900	5436	1.6	-7.9	5229	1.6	-11.4
Ta	-	-	-	-	0.028	0.012	21.7	-57.7	0.003	0.007	39.5	142	Ta	0.500	0.45	15.9	-9.2	0.49	5.6	-1.5
Pb	-	-	-	-	0.036	0.231	25.8	540.5	0.004	0.317	24.5	8473	Pb^{208}	2.52	2.59	11.5	2.9	1.96	4.6	-
Th	-	-	-	-	0.0094	0.0102	14.0	8.9	0.0014	0.0014	52.9	-2.8	Th	30.0	29.4	4.7	-1.8	23.3	4.1	-22.2
U	-	-	-	-	0.0030	0.0029	21.6	-3.2	0.0026	0.0023	30.6	-10.4	U	80.0	80.3	5.5	0.3	58.2	4.6	-27.3

Reference values are from GeoReM; Rep.rate: Repetition rate; Crater dia.: Crater diameter; Ref.: Reference; AVG: Average; SD%: percent one standard deviation; RD%: percent relative deviation; C.F.: Correction factor. Total Fe reported as FeO. Pb in 91500 was reported by ^{208}Pb as Pb isotope ratios are greatly different from SRM610, ΣTrOx.: total oxide wt.% of trace elements analyzed

ESI Data 5

Table 1. Relative fractionation factor (%RD) from the reference values of the analyzed samples.

Element	block	MP(°C)	193Ex[1]	193Ex[2]	193Ex[3]	200Fs[1]	Fs-Ex[1]
Experiment #			A	B	C	D	E
Si	p	1412	-3.4	2.1	-17.0	-2.8	20.2
Ti	d	1666	20.4	4.1	-0.8	20.0	-7.0
Al	p	660	8.1	0.9	-8.0	-1.0	-14.4
Fe	d	1536	3.5	-0.1	15.4	25.8	0.6
Mn	d	1246	-1.4	-8.4	10.0	-10.5	20.9
Mg	s	650	1.9	20.3	1.0	4.5	-17.0
Ca	s	842	1.1	-11.8	-0.8	-16.9	0.5
Na	s	98	-8.5	0.7	–	-13.8	5.4
K	s	64	-37.8	7.3	–	29.7	-24.0
P	p	44	-35.1	-9.4	–	-47.8	14.8
Sc	d	1539	4.0	-10.2	6.4	-15.9	-5.6
V	d	1917	5.0	-1.0	–	-3.5	12.2
Cr	d	1856	4.8	-8.9	11.8	-2.1	24.7
Co	d	1495	2.4	5.4	–	4.2	25.3
Ni	d	1455	5.0	5.2	22.6	19.6	29.4
Cu	d	1085	-16.0	0.5	28.0	-3.5	38.2
Zn	d	420	-12.5	2.1	42.4	-4.7	21.2
Rb	s	39	2.7	2.2	–	-1.3	13.8
Sr	s	777	0.1	-11.7	–	-14.0	-7.6
Y	d	1520	-11.0	-18.9	6.4	-27.1	-18.5
Zr	d	1852	-13.6	-15.0	8.2	-26.0	-10.6
Nb	d	2985	1.8	-11.3	–	-11.9	-0.6
Ba	s	729	1.1	-8.1	-15.2	-14.9	4.9
La	f	920	-2.4	-11.7	-9.8	-18.4	-1.7
Ce	f	799	1.3	-11.6	-11.6	-17.1	11.6
Pr	f	935	-3.3	-14.5	–	-21.2	-3.7
Nd	f	1024	-2.5	-13.8	-18.8	-21.7	-6.1
Sm	f	1072	-3.2	-17.2	-20.6	-19.7	-5.7
Eu	f	826	-1.2	-16.4	-22.4	-18.1	-7.6
Gd	f	1312	-8.6	-16.2	-18.8	-26.3	-13.5
Tb	f	1356	-11.4	-24.7	-24.2	-25.0	-13.0
Dy	f	1407	-8.4	-15.5	-22.4	-21.9	-13.4
Ho	f	1461	-10.4	-15.0	-20.6	-22.8	-14.6
Er	f	1522	-13.7	-14.6	-18.8	-29.3	-11.0
Tm	f	1545	-7.2	-15.8	-20.6	-30.9	-5.8
Yb	f	824	-4.6	-14.8	-24.2	-20.8	-5.0
Lu	f	1652	-9.0	-20.3	-26.0	-28.2	-7.7
Hf	d	2150	-15.1	-19.4	-27.8	-31.0	-3.8
Ta	d	2985	0.9	-12.8	-22.4	-17.5	3.6
Pb	p	328	-8.7	-16.1	-18.8	-11.9	23.4
Th	f	1750	-4.0	-12.4	-17.0	-20.8	2.2
U	f	1132	-14.1	-3.5	-14.3	-17.0	14.0

Ex: excimer, Fs: femtosecond, References: [1]: This study, [2]: Liu et al. (2008), [3]: Kroslakova & Günther (2007). MP: melting point of element (°C), Experiment# correlate those in Fig. 2.

Table 2. Regression curve parameters and correlation coefficients between %RD and melting point of rare earth elements.

Laser type	Exp.#	Standard	Sample	a	b	r^2
193Ex[1]	A	SRM610	Basalt	-0.0131	-7.25	0.7876
193Ex[2]	B	SRM610	Basalt	-0.0137	-4.6947	0.6704
193Ex[3]	C	SRM610+Rb	SRM610	-0.0100	-6.6644	0.2197
200Fs[1]	D	SRM612	Basalt	-0.0128	9.283	0.7794
Fs-Ex[1]	E	612-266Fs	612-193Ex	-0.0155	11.852	0.4731

Ex: excimer, Fs: femtosecond, Bas: Basalt, +Rb: Rb addition through ARIDUS, a and b: linear regression parameters for %RD = a X + b where X = melting point (°C) of REE, r^2: regression coefficient, References: [1]: This study, [2]: Liu et al. (2008), [3]: Kroslakova & Günther (2007), Exp.# correlate those in Fig. 2.

ESI Data 5 Table 3. Relative fractionation factor ($D(\%RD)_{Ref.line}$) from the REE reference line of the analyzed samples.

Element	block	FIE	193Ex[1]	193Ex[2]	193Ex[3]	200Fs[1]	Fs-Ex[1]
Experiment #			A	B	C	D	E
Si	p	786.5	22.9	5.4	26.7	3.8	30.3
Ti	d	658.8	49.1	32.5	10.9	22.5	7.0
Al	p	277.5	14.9	7.2	11.7	5.3	-16.0
Fe	d	762.5	53.2	13.9	23.5	37.4	12.6
Mn	d	717.3	13.1	5.3	23.3	29.1	28.4
Mg	s	737.3	20.3	0.9	6.6	14.2	-18.8
Ca	s	589.8	1.4	2.6	4.9	14.3	1.8
Na	s	495.8	-5.3	-16.5	3.8	7.6	-5.0
K	s	418.8	37.8	-46.3	13.4	7.3	-34.8
P	p	1011.8	-39.9	-43.8	-3.7	7.1	3.7
Sc	d	633.1	11.5	14.4	-0.8	28.5	6.5
V	d	650.9	28.9	20.2	26.6	25.8	30.2
Cr	d	652.9	29.5	19.3	23.9	37.0	41.7
Co	d	760.4	31.0	12.3	28.3	21.6	36.7
Ni	d	737.1	45.9	14.3	30.9	43.8	40.1
Cu	d	745.5	18.0	-11.4	17.9	45.5	43.2
Zn	d	906.4	8.1	-16.4	13.1	53.3	15.9
Rb	s	403.0	6.4	-6.1	8.0	7.1	2.6
Sr	s	549.5	3.5	0.8	2.5	14.4	-7.4
Y	d	600.0	0.1	-0.8	-4.1	28.3	-6.7
Zr	d	640.1	5.6	0.8	6.8	33.4	6.3
Nb	d	652.1	34.4	30.8	16.8	36.5	33.9
Ba	s	502.9	1.9	1.1	0.6	-1.2	4.3
Hf	d	658.5	4.4	3.2	15.1	0.4	17.7
Ta	d	761.0	28.9	29.9	21.6	14.1	38.1
Pb	p	715.6	-0.3	-13.7	-5.6	-8.8	16.6
Th	f	587.0	9.4	9.1	11.7	7.2	17.6
U	f	597.6	5.0	-8.9	15.6	3.7	19.7

Ex: excimer, Fs: femtosecond, References: [1]: This study, [2]: Liu et al. (2008), [3]: Kroslakova & Günther (2007). FIE: first ionization energy of element (kJ/mol), Experiment# correlate those in Fig. 2. REEs are not shown as they are used as normalization reference line.

Table 4. Apparent ionization temperature of standards (Ta(sd)) calculated based on Saha's equation.

Element	block	FIE	193Ex[1]	193Ex[2]	193Ex[3]	200Fs[1]	Fs-Ex[1]
Experiment #			A	B	C	D	E
Si	p	786.5	6124	6082	6507	6452	6046
Ti	d	658.8	5080	5550	5316	5203	5696
Al	p	577.5	4848	4921	5180	5076	–
Fe	d	762.5	5741	5985	5847	6135	6163
Mn	d	717.3	5889	5707	5637	6157	5645
Mg	s	737.7	5881	6208	5989	6570	–
Ca	s	589.8	5734	5302	4954	5522	5656
Na	s	495.8	–	–	–	–	–
K	s	418.8	–	–	–	–	–
P	p	1011.8	6913	6696	6652	6948	6665
Sc	d	633.1	5346	–	5061	5272	5535
V	d	650.9	5183	5209	5218	5294	5170
Cr	d	652.9	5192	5256	5123	5322	5087
Co	d	760.4	5890	5918	5998	6159	5840
Ni	d	737.1	5626	5748	5640	5983	5667
Cu	d	745.5	5965	5967	5682	–	5698
Zn	d	906.4	6613	6577	6380	6879	6559
Rb	s	403.0	–	–	–	–	–
Sr	s	549.5	5100	5210	–	5651	–
Y	d	600.0	6585	–	4825	–	–
Zr	d	640.1	5638	5570	5063	6248	5598
Nb	d	652.1	5139	5361	5121	5172	5143
Ba	s	502.9	4921	5324	–	5103	–
Hf	d	658.5	5848	5442	6494	5954	5390
Ta	d	761.0	5915	6002	6124	5905	5832
Pb	p	715.6	6755	–	–	–	5802
Th	f	587.0	5065	4994	5152	5074	4870
U	f	597.6	5352	4985	5459	–	4914

Ex: excimer, Fs: femtosecond, References: [1]: This study, [2]: Liu et al. (2008), [3]: Kroslakova & Günther (2007). FIE: first ionization energy of element (kJ/mol), Experiment# correlate those in Fig. 2. REEs are not shown as they are used as normalization reference line.

Table 5. Regression curve parameters and correlation coefficients between first ionization energy (FIE) and apparent ionization temperature of elements in samples Ta(sd) (K).

Element type	a	b	r^2
s-block	4.65	2722	0.652
p-block	3.96	2888	0.892
d-block	5.20	1959	0.792
f-block (Th, U)	N/A	N/A	N/A
All	4.28	2649	0.779

Ex: excimer, Fs: femtosecond, Bas: Basalt, +Rb: Rb addition through Aridus, a and b: linear regression parameters for Ta(sd) = a X + b where Ta(sd) = apparent ionization T (K) in standards and X = FIE (kJ/mol), r^2: regression coefficient. Note that the regression lines are obtained from all dataset in five different experiments shown in Table 3. Th and U have a narrow FIE variation and REEs are used for previous normalizations, so that these elements are not used for calculations.